Scilight

Bulletin of Computational Intelligence
https://www.sciltp.com/journals/bci

Article

An Efficient Meta-Ensemble Paradigm for Modelling Poisson's Ratio and Maximum Horizontal Stress in Casing Collapse Hazard

Abidhan Bardhan [1,*] and Navid Kardani [2]

[1] Department of Civil Engineering, National Institute of Technology Patna, Patna 800005, India
[2] Software Technical Lead, ITW Construction-Asia Pacific, Chirnside Park 3116, Australia
* Correspondence: abidhan@nitp.ac.in

How To Cite: Bardhan, A.; Kardani1, N. An Efficient Meta-Ensemble Paradigm for Modelling Poisson's Ratio and Maximum Horizontal Stress in Casing Collapse Hazard. *Bulletin of Computational Intelligence* **2026**, *2*(2), 146–163. https://doi.org/10.53941/bci.2026.100008

Received: 17 December 2025
Revised: 21 February 2026
Accepted: 17 March 2026
Published: 3 April 2026

Abstract: This study develops an efficient meta-ensemble paradigm for predicting geotechnical-geological parameters namely static Poisson's ratio (PR) and maximum horizontal stress (MHS) significant to casing collapse hazards. Engineers strive to reduce the risk of casing collapse due to drilling through the meticulous design of wells and operation practices. Thus, identifying casing collapse hazards in oil and gas wellbores necessitates a thorough geotechnical examination. For this purpose, a stacking ensemble paradigm was developed to predict PR and MHS, the two most important variables of casing collapse hazards. Three conventional models (viz., gradient boosting regressor, decision tree regressor, and k-nearest neighbour regressor) and linear regressor were used as base models to construct a stacking ensemble paradigm (ENSM) in which a random forest regressor was used as the meta-model. The performance of the ENSM model was compared with two additional standalone models namely feed-forward neural network and extreme learning machine. Experimental results exhibit that the ENSM paradigm delivers higher prediction accuracy than all other employed models with R^2 values ranging from 0.9755 to 0.9991. The experimental results confirmed that the proposed ENSM paradigm achieves high prediction accuracy in predicting the PR and MHS of soils and can be considered an effective approach to aid engineers in assessing the risk of casing collapse hazards in oil and gas wellbores and operation practices.

Keywords: wellbore casing collapse; geological sub-surface model; applied geophysics; ensemble machine learning model; artificial intelligence

1. Introduction

Despite significant advancements in drilling technologies, the extraction of oil and gas from subterranean reservoirs in many global locations continues to be a challenging, costly, and hazardous endeavour. The primary challenges arise from uncertainty pertaining to the underground stress fields and their impact on the rock strata that must be traversed to successfully reach and exploit productive reservoirs. The areas of a wellbore that are susceptible to drilling difficulties are typically characterized by changing tectonic forces, aberrant pressure zones, poorly consolidated material, and weak formations. In many scenarios, achieving continuous drilling from a surface to a target reservoir in a stable wellbore condition with a uniform-gauge hole size is highly challenging. Consequently, drilling engineers are required to strategically plan and execute the construction of a wellbore in discrete sections. These sections are fortified with a robust steel pipe, referred to as casing, which possesses a substantial diameter. Additionally, the casing is firmly secured and interconnected with the surrounding rock

Copyright: © 2026 by the authors. This is an open access article under the terms and conditions of the Creative Commons Attribution (CC BY) license (https://creativecommons.org/licenses/by/4.0/).
Publisher's Note: Scilight stays neutral with regard to jurisdictional claims in published maps and institutional affiliations.

formations through the application of a cement sheath. This cement sheath serves the crucial purpose of establishing a reliable high-pressure seal [1,2].

The drilling process of oil and gas wells, particularly in deep and ultra-deep wells, presents challenges related to well completion, production, complicated strata, and operating modes. This leads the oil and gas well casings being exposed to complex load conditions, including irregular borehole-induced uneven stratum rheology [3,4], water absorption-induced mudstone expansion [5], stratum subsidence, slip [6], and casing eccentricity and cement quality [7]. These factors collectively result in abnormally significant non-uniform extrusion effects on the oil and gas well casings. Therefore, the occurrence of oil and gas well casing collapse failure is highly possible, causing a variety of adverse consequences, such as frequent workovers, liner, and tubing damage-induced production reductions, the potential for oil and gas leakage to the surface, and ultimately, the probability of losing control over the well [8].

It has been shown that the natural and structural features of rock layers are linked to one of the key mechanisms leading to the oil and gas well casing collapse in wellbores. Creep is a factor affecting the gradual deformation of layers over time. In the realm of long-term creep phenomena, salt and clay-rich shale represent two particularly formidable geological strata [9,10]. The cement sheath and the well casings are subjected to compressional and shear stresses by these movements, in some cases so severe that they may lead to the collapse of well casings [11]. Poisson's ratio (PR) is regarded as a useful criterion often used to express the ability of such materials to deform when subjected to pressure. However, the maximum horizontal stress (MHS) is a useful criterion used to express the disruptive force of the stresses affecting the oil and gas well casing-protected wellbores from the underground stress field. Consequently, the emphasis of this machine learning analysis is on the accurate estimation of these two variables.

Wang and Samuel [10] examined the effects of salt creep behaviour on wellbore casing using a three-dimensional finite element model (FEM) with rheological constitutive equations. Willson et al. [3] investigated the oil and gas well casing loads in uncemented borehole sections using a novel numerical model. Tong et al. [12] examined the effects of salt creep on casing-bearing strength using a two-dimensional FEM that included the salt structure deformation and a multistep coupling FEM. Hedayatikhah and Abdideh [13] used a FEM to analyse well geo-mechanical data in the Marun oil field. Salehi et al. [14] investigated the collapse in the oil and gas well casings using an artificial neural network (ANN), considering different broad potentially effective variables, such as latitude, longitude, total well depth, corrosion factor, time and collapsed zone details. Mohamadian et al. [2] studied the prediction of collapse in the oil and gas well casings using two hybrid neural network models constructed using particle swarm optimization and genetic algorithm. Other machine learning algorithms (MLAs) used in casing failure modeling and the estimation of well casing collapse in oil and gas wells include random forest, gradient boosting, and so on [15–17].

Nonetheless, as per the existing literature, it becomes apparent that there is a scarcity of experiments that have explored the potential of ensemble learning algorithms in predicting collapse in gas and oil well casings. Notably, there has been a resurgence of interest in the application of ensemble learning methodologies within the domains of engineering and sciences in recent years. Moreover, ensemble learning algorithms have the advantage of being data-driven and self-adaptive, and they can learn to characterize predictive models concerning a given dataset. Besides, it has been proven that such techniques can solve a variety of problems in different disciplines [18–22]. Several researchers use ensemble learning techniques in civil engineering fields including geotechnical and geological engineering [23–25], slope stability [26], construction and building materials [27–30], and sub-grade modelling [31], and found notable results.

This study utilizes a stacking ensemble (ENSM) paradigm for the estimation of PR and MHS in the collapse evaluation of oil and gas well casings. The stacking is a commonly employed technique in ensemble learning. It involves utilizing predictions generated by various MLAs, referred to as base learners, as inputs for a secondary learning algorithm known as the meta-model. In this study, linear regressor (LR), gradient boosting regressor (GBR), decision tree regressor (DTR), and K-nearest neighbour regressor (KNR) were used as the base learners in the first layer, whereas random forest regressor (RFR) was used as the meta-model in the second layer. This stacking ensemble approach has been designated as the ENSM paradigm. The robustness of the proposed ENSM paradigm was also evaluated in comparison to the performance of base learning separately and two other standalone models including a feedforward neural network (FFNN) and extreme learning machine (ELM).

The subsequent sections of this study are structured in the following manner. Section 2 provides the research significance, while Section 3 offers an overview and methodological description of the models that were utilized in the study. The data description is provided in Section 4, followed by the presentation of results and subsequent discussions in Section 5. Section 6 concludes the discussion by providing a summary and conclusions.

2. Research Significance

Over the past two decades, there has been a significant proliferation of modern machine learning models that have been introduced and widely employed. These inventions have been developed with the objective of forecasting the outcomes of different tasks in the domain of engineering and sciences [32–35]. The observed events demonstrate significant non-linear properties and behaviors, making it difficult to rely on deterministic methodologies traditionally used. However, in recent times, there has been an increased interest in the utilization of ensemble learning approaches in the field of engineering and sciences [20–22,36]. Nevertheless, existing research in the field of geo-mechanical sub-surface modelling lacks sufficient application of ensemble learning modelling using a meta-model-based stacking ensemble approach. Thus, this research presents an ENSM approach constructed using RFR as a meta-model for the estimation of PR and MHS in casing collapse hazard.

3. Methodology

This section presents methodological details of the employed paradigms, including FFNN, ELM, LR, GBR, DTR, and KNR. Notably, a brief overview is presented for these algorithms. In addition, the methodological development of the stacking ENSM paradigm using RFR is presented.

3.1. Brief Details of Standalone Models

ANN is a prevalent soft computing framework derived from the principles of human brain functioning. ANNs employ multiple layers of mathematical processing to acquire knowledge from observed data. One of the classical types of ANNs is the feedforward neural network (FFNN). FFNN is like ANN with three layers, including an input, a hidden, and an output layer. It is a network where no cycles are generated by inter-node connections. FFNNs are the most basic networks that process data in just a single direction. While data can travel through multiple hidden nodes, they only flow in a single direction, with no backward data movement. FFNNs are used in data-driven modelling owing to their simplified and straightforward structure. Previous research has gone into more detail about FFNNs and their applications [37,38].

ELM is also a widely used soft computing framework which comes under the neural network category. ELM has only one layer of hidden neurons and hence called a single-layer feedforward network (SLFN). The output weights of ELM are determined based on the least squares method, given that the biases and weights of the hidden layer are already established. Unlike traditional FFNNs, ELMs employ a continuous probability distribution function in lieu of iterative solutions for their operations. ELM has a lower complexity in design and can solve regression and classification problems more quickly. Consequently, iterative training techniques that decompose estimation data into local minima rather than global minima are no longer needed. Details of the mathematical background of ELMs can be seen in the original study of Huang et al. [39].

One of the most significant, simplest, and frequently used regression techniques is LR. In general, there are two types of LR, including simple linear and multiple linear regression. When doing LR of some dependent variable y to a series of independent variables $x = (x_1, \dots, x_r)$, where r indicates the number of predictors, a linear relationship can be assumed between y and x: $y = \beta_0 + \beta_1 x_1 + \cdots + \beta_r x_r + \varepsilon$, called the regression equation. where $\beta_0, \beta_1, \dots, \beta_r$ indicate the regression coefficients and ε indicate the bias or error term. LR models the estimators of the regression coefficients or simply the predicted weights, represented by $b_0, b_1, \dots, b_r$. They characterize $f(x) = b_0 + b_1 x_1 + \cdots + b_r x_r$ as the estimated regression equation, which should be able to accurately evaluate the dependencies between the inputs and output variables [39].

GBR is a widely used MLA that utilizes an ensemble approach by integrating fundamental models into a unified composite model. Boosting is referred to as an additive model due to the sequential introduction of basic models, also known as weak learners, while keeping the trees in the model constant. A more robust predictive capability can be attained through the integration of more foundational models. The term "gradient boosting" pertains to the utilization of gradient descent by the algorithm to minimize losses. Gradient boosting employs decision trees as weak learners, with a squared error loss function. Subsequently, a suboptimal model is trained using GBR to establish a mapping between the features and the residuals projected by a weak model. These residuals are subsequently included into the input of the existing model; hence, facilitating the model's alignment with the desired target. The overall predictive efficiency of the model is improved as this step is repeated continuously [8].

DTR is also a widely employed MLA in solving regression-based problems. During the training phase, the input variable(s) are assigned specific values that are considered by a particular function. The process by which a decision tree (DT) is generated from specific cases is commonly known as the stimulus for the DT. The technique aims to identify optimal DTs by minimizing the fitness function. The objective of the DTR is to forecast a

continuous target variable, as opposed to a categorical one. This characteristic renders it highly advantageous in situations when predictions are required based on several input features. The decision-making process within a DTR entails iteratively partitioning the dataset into subgroups, utilizing the feature that yields the most optimal division. This determination is often made by evaluating metrics such as mean squared error or variance reduction. The iterative procedure persists until a predetermined stopping condition is satisfied. Although DTRs are prone to overfitting if not appropriately controlled, they are highly regarded for their capability to handle both numerical and categorical data [40–42].

KNR is a simple method that stores all potential scenarios and makes predictions for numerical targets based on a similarity measure, such as distance functions. The KNR approach has been employed as a non-parametric tool in statistical estimations and pattern recognition. The computation of the mean value of the numerical goal in the KNR is a simple and direct application of the KNN algorithm. Another strategy that can be used is the calculation of an inverse distance weighted average of the K nearest neighbors. KNR uses the same distance functions as KNN classification, i.e., Euclidean distance. It is best to inspect the data before deciding on the best value for K. Although a high value of K is more accurate as it decreases the total noise, it comes at the cost of blurring the different boundaries within the feature space [43].

3.2. Stacking Ensemble Model

The ensemble systems, as a mixture of experts, are defined as meta-algorithms combining many standalone MLAs (called base models) into one predictive model. Researchers have recently discovered various benefits of ensemble approaches in automated decision-making applications, particularly in the field of engineering. It is undeniable from a statistical standpoint that the acceptable efficiency of regressors on the training dataset does not imply an excellent efficiency on data not seen during the training phase. This indicates that even if the testing dataset is not a fair representation of potential field data, machine-learning algorithms with the same generalisation efficiencies will have various predictive efficiencies.

In the stacking technique, multiple MLAs are employed as base models. However, an additional layer of the model, known as the meta-model, is also incorporated. In contrast to voting ensembles, this model employs distinct weight assignments for the base models and thereafter conducts the prediction task by stacking. Suppose there are four base models, namely LR, GBR, DTR, and KNR, and the meta-model in the second layer is the RFR. Now, to train the base models, a dataset should be given as input to every respective base model. After training the base models, the prediction data should be used to train the meta-model, RFR. Thus, the training data for the RFR will be different. Upon the introduction of the meta-model, it will allocate weights to the base models, resulting in the output of the base models being deemed as the ultimate output of the stacking algorithm. An illustration of the concept is presented in Figure 1. As discussed above, the proposed stacking ENSM framework incorporates LR, GBR, DTR, and KNR as base models, while the RFR functions as the meta-model.

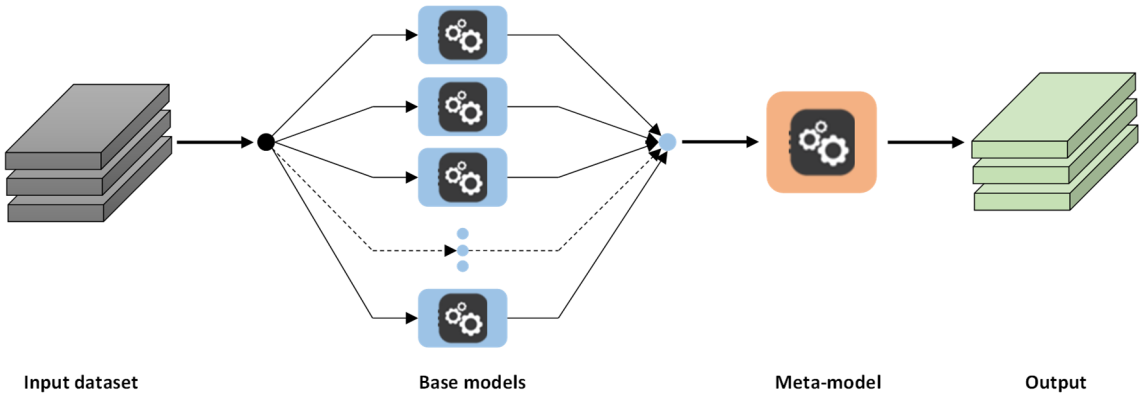

Figure 1. Flow chart showing the working principle of sa tacking ensemble model.

3.3. Overall Methodology

Figure 2 presents the overall methodology of the presented study. Notably, after data collection, four base models, namely LR, GBR, DTR and KNR, were used to predict the PR and MHS parameters. Subsequently, these base models were integrated using a stacking ensemble paradigm (ENSM), in which the RFR was employed as the meta-model to generate the final predictions. Finally, the performance of all the models, i.e., LR, GBR, DTR and KNR, FFNN, ELM, and ENSM, was compared and discussed.

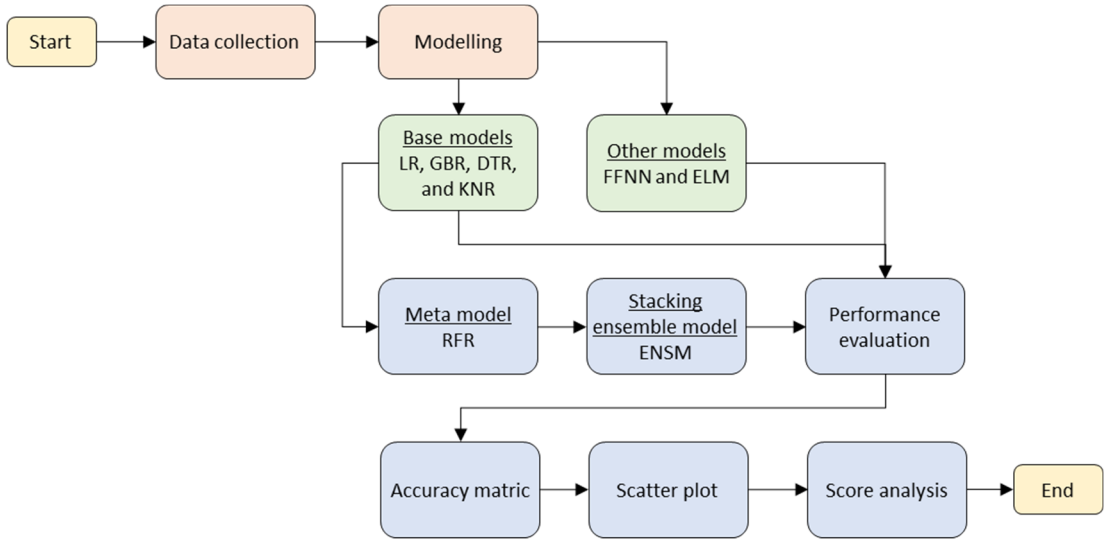

Figure 2. Flow chart showing the overall methodology.

4. Data Description and Performance Assessment

A total of 22,323 data was collected from the work of Mohamadian et al. [2], consisting of five influential variables, including well depth (D in m), compressional wave velocity (DTC in μs/ft), shear wave velocity (DTS in μs/ft), bulk density (RHOB in g/cm^3), and pore pressure (PP in MPa). These variables were used as inputs to estimate PR (in -) and MHS (in psi) of soils in the oil and gas well casings. Descriptive statistics of the collected dataset are tabulated in Table 1. According to the table, the parameter D lies in the range of 1993.01 m to 3693.95 m. The minimum and maximum values of DTC and DTS are 43.54 μs/ft, 95.75 μs/ft and 91.44 μs/ft, and 157.34 μs/ft, respectively. Similarly, the minimum and maximum values of RHOB and PP are 1.73 g/cm^3, 77.34 MPa and 3.02 g/cm^3, 80.71 MPa, respectively. The output parameters PR and MHS are fall in the range of −0.23 to 0.43 and 13,162.18 psi to 22,212.32 psi. The standard error values suggest that the gathered dataset exhibits minimal associated error, while the variance values indicate that the dataset encompasses a broad range of variables.

Table 1. Statistical summary of the variables.

Parameters	D	DTC	DTS	RHOB	PP	PR	MHS
	(m)	(μs/ft)	(μs/ft)	(g/cm^3)	(MPa)	(-)	(psi)
Minimum	1993.01	43.54	95.75	1.73	77.34	−0.23	13,162.18
Mean	2843.48	66.46	118.95	2.31	77.71	0.26	15,935.46
Maximum	3693.95	91.44	157.34	3.02	80.71	0.43	22,212.32
Stnd. Error	3.29	0.05	0.06	0.00	0.01	0.00	10.81
Stnd. Deviation	491.05	7.53	9.26	0.30	0.83	0.07	1614.49
Variance	241,131.12	56.63	85.78	0.09	0.70	0.01	2,606,592.32
Kurtosis	−1.20	0.38	1.23	−0.46	2.87	1.79	0.99
Skewness	0.00	0.02	0.16	0.87	2.04	−1.45	1.22

However, to better demonstrate the gathered dataset, the Pearson correlation matrix and comparative frequency histogram are illustrated in Figures 3 and 4, respectively. According to the figures, the maximum negative correlation of −0.78 was found between DTC and MHS and −0.71 between DTC and PR. Similarly, the maximum positive correlation of 069 was found between RHOB and MHS and 0.11 between DTS and PR. The output parameters PR and MHS are positively correlated with R = 0.44, where R = degree of correlation. It is seen that MHS exhibits higher correlations with influential variables as compared to the correlations between PR and the same variables. Also, there is no significant correlation between the inputs and outputs, meaning that conventional learning methods, such as LR, are unable to simulate the nonlinear relationships between inputs and outputs, and nonlinear regression might produce better results. Contrarily, Figure 4 presents a comparative frequency histogram with data distribution from which the data range and distribution can be visualized. Notably, normalized values of variables were considered for this figure.

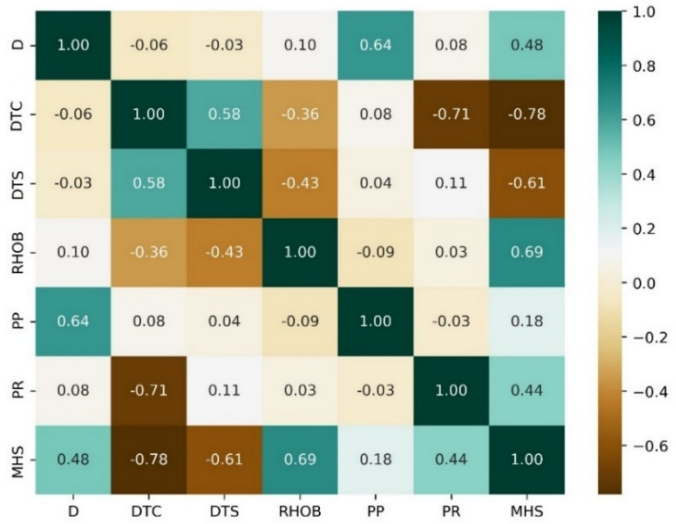

Figure 3. Correlation matrix of the input and output variables.

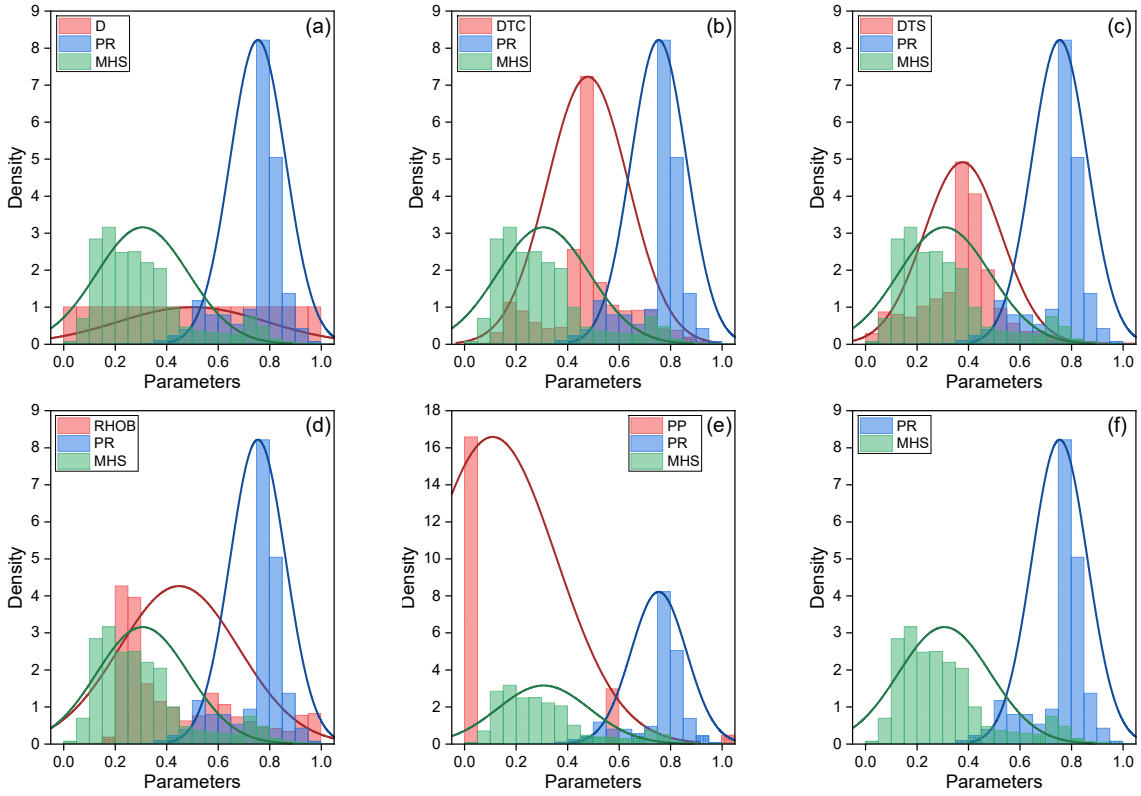

Figure 4. Comparative frequency histogram with data distribution (based on normalized values) for (**a**) D, (**b**) DTC, (**c**) DTS, (d) RHOB, (**e**) PP, and (**f**) output parameters.

In the domains of soft computing, data normalization is a pre-processing task which helps in adjusting the dimensionality effects of the variables under consideration. Thus, until the model is generated, all the variables are normalized in the range of 0 to 1 using the min-max approach. Notably, the main dataset was separated into training and testing subsets with a 70:30 ratio. The training subset (i.e., 70% of the main dataset) was used for model construction while the balance 30% dataset, called testing dataset, was used for model validation. Specifically, 70% (i.e., 15,626 samples) and 30% (i.e., 6697 samples) of data were used as the training and testing datasets for the construction and validation of FFNN, ELM, LR, GBR, DTR, KNR, and ENSM models, respectively. During model training and testing, the values of MHS were multiplied by a factor of 0.001 to reduce overfitting. Therefore, all the estimated values of MHS should be multiplied by 1000 after de-normalization to get the actual estimated values. It is also mentioned that a model constructed and validated using a large sample can be considered appropriate. Given the substantial number of samples used for both training and testing, the constructed models can be considered statistically reliable and robust. Figure 5 illustrates the steps of computational modelling.

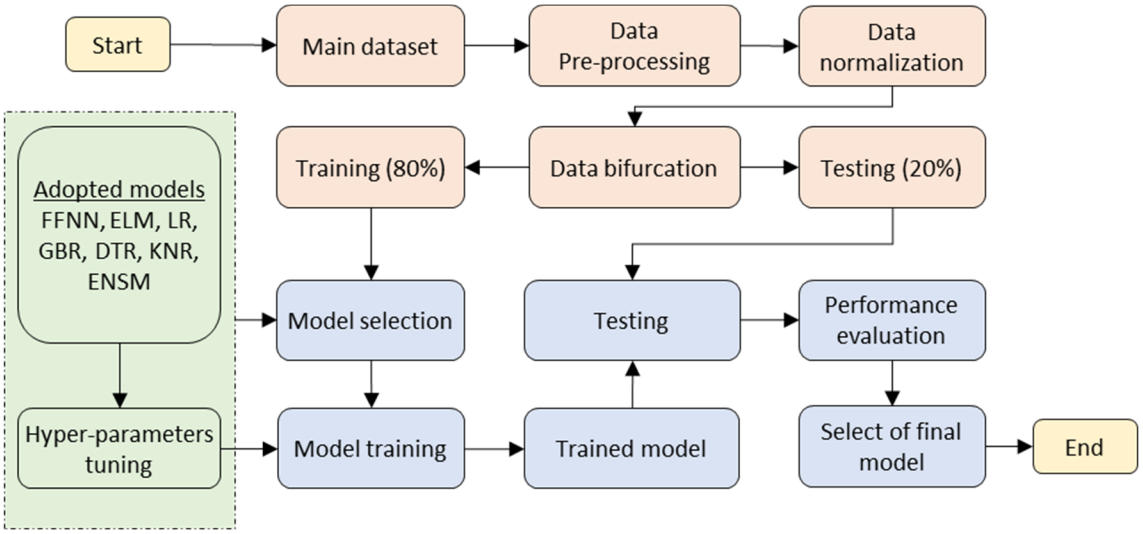

Figure 5. Illustration of computational modelling.

After the model construction, seven widely used performance indices namely coefficient of determination (R^2), Willmott's index of agreement (WI), Nash-Sutcliffe efficiency (NSE), root mean squared error (RMSE), mean absolute error (MAE), RMSE to observation's standard deviation ratio (RSR), and weighted mean absolute percentage error (WMAPE), were assessed to investigate model performance. Notably, multiple indices were used to assess model performance from different perspectives, including amount of correlation, the degree of associated error, the weighted error, and so on. Mathematical expressions of these indices are given by:

$$R^2 = \frac{\sum_{i=1}^{n}(y_i - y_{mean})^2 - \sum_{i=1}^{n}(y_i - \hat{y}_i)^2}{\sum_{i=1}^{n}(y_i - y_{mean})^2} \tag{1}$$

$$WI = 1 - \left[\frac{\sum_{i=1}^{n}(y_i - \hat{y}_i)^2}{\sum_{i=1}^{n}\{|\hat{y}_i - y_{mean}| + |y_i - y_{mean}|\}^2}\right] \tag{2}$$

$$NSE = 1 - \frac{\sum_{i=1}^{n}(y_i - \hat{y}_i)^2}{\sum_{i=1}^{n}(y_i - y_{mean})^2} \tag{3}$$

$$RMSE = \sqrt{\frac{1}{n}\sum_{i=1}^{n}(y_i - \hat{y}_i)^2} \tag{4}$$

$$MAE = \frac{1}{n}\sum_{i=1}^{n}|(\hat{y}_i - y_i)| \tag{5}$$

$$RSR = \frac{RMSE}{\sqrt{\frac{1}{n}\sum_{i=1}^{n}(y_i - y_{mean})^2}} \tag{6}$$

$$WMAPE = \frac{\sum_{i=1}^{n}\left|\frac{y_i - \hat{y}_i}{y_i}\right| \times y_i}{\sum_{i=1}^{n} y_i} \tag{7}$$

where y_i and $\hat{y}_i$ are the actual and predicted ith value, n is the number of data samples in a dataset, and y_{mean} is the average of the actual values.

5. Results and Discussions

Emphasizing that the selection of an optimal prediction model necessitates the proper adjustment of hyper-parameters of the employed models is crucial. This is primarily because each algorithm has a unique set of hyper-parameters that affect the efficacy of a model. Consequently, various sets of hyper-parameters were utilized to evaluate the performance of the implemented models; the details of which are provided below. The subsequent

subsections also provide an analysis and presentation of the performance of the utilized models (i.e., FFNN, ELM, LR, GBR, DTR, KNR, and ENSM) for the estimation of PR and MHS in casing collapse hazard.

5.1. Model Configuration and Performance

As stated above, a total of 22,323 data was collected from the work of Mohamadian et al. [2], consisting of five influential variables. Subsequently, the training subset (i.e., 15,626 cases) was applied to train the models and the testing dataset (i.e., 6697 cases) was used to evaluate their robustness. FFNN with single hidden layer, the optimum number of hidden neurons (N_{Hopt}) was determined to be 11. The optimal predictive precision for ELM was achieved with N_{Hopt} = 12. Contrarily, n_estimators was set to 100 for GBR, max_depth of GBR and DTR was set to 3 and 10, respectively, and for KNR, n_neighbors was set to 10. The proposed stacking ENSM model was constructed using LR, GBR, DTR and KNR as base models and the RFR as the meta-model. An illustration of the proposed ENSM paradigm is presented in Figure 6.

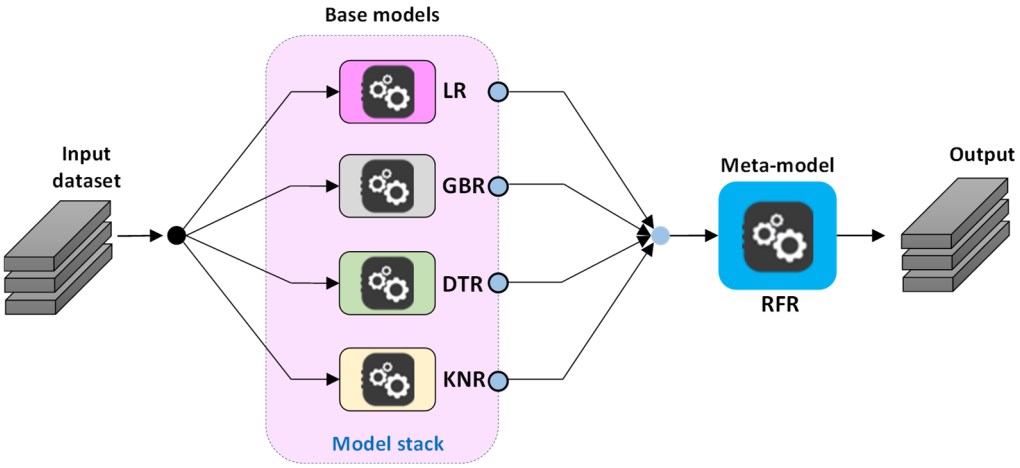

Figure 6. Illustration of the propped stacking ENSM paradigm.

Notably, three-fold cross-validation (CV-1, CV-2, and CV-3) was performed in this study to select the most suitable testing subset. As stated above, the main dataset was partitioned into training and testing subsets with 70% and 30% ratio. Thus, a sum of 6697 datasets was selected at random to select three cross-validation sets. The results of cross-validation (based on the RMSE value) are presented in Table 2. Based on the results, the testing set of the CV-1 was used for further model validation. The outcomes of the developed/employed models are tabulated in Tables 3–6. The outcomes of PR estimation for the training (TR) and testing (TS) subsets are displayed in Tables 3 and 4, respectively, whereas the results of MHS estimation are presented in Tables 5 and 6 for the same subsets. The maximum prediction accuracy was achieved by the stacking ENSM for both PR (training phase: R^2 = 0.9855 and RMSE = 0.0130; testing phase: R^2 = 0.9755 and RMSE = 0.0171) and MHS (training phase: R^2 = 0.9991 and RMSE = 0.0055 psi; testing phase: R^2 = 0.9985 and RMSE = 0.0068 psi) estimation in casing collapse hazard. Also, the R^2 index indicates that the developed/utilized paradigms exhibit accuracy values ranging from 0.9101 to 0.9855 for the training subset and 0.9072 to 0.9755 for the testing subset of PR estimation. Similarly, the R^2 indices for the training subset and testing subset of the MHS estimation range from 0.9687 to 0.9991 and 0.9675 to 0.9985, respectively.

Table 2. Results of cross-validation based on the RMSE value.

Models	PR			MHS		
	CV-1	CV-2	CV-3	CV-1	CV-2	CV-3
FFNN	0.0256	0.0272	0.0285	0.0137	0.0143	0.0145
ELM	0.0284	0.0299	0.0306	0.0084	0.0096	0.0094
LR	0.0333	0.0349	0.0352	0.0318	0.0318	0.0323
GBR	0.0248	0.0256	0.0267	0.0131	0.0133	0.0131
DTR	0.0212	0.0183	0.0186	0.0156	0.0132	0.0134
KNR	0.0202	0.0211	0.0226	0.0079	0.0084	0.0081
ENSM	0.0171	0.0177	0.0185	0.0068	0.0073	0.0070

Note: CV-1 = Cross-validation part 1, CV-2 = Cross-validation part 2, CV-3 = Cross-validation part 3.

Table 3. Results for the training dataset (PR estimation).

Index/Particulars		FFNN	ELM	LR	GBR	DTR	KNR	ENSM
R^2	V	0.9480	0.9367	0.9101	0.9559	0.9842	0.9730	**0.9855**
	S	3	2	1	4	6	5	**7**
WI	V	0.9865	0.9834	0.9759	0.9884	0.9960	0.9930	**0.9963**
	S	3	2	1	4	6	5	**7**
NSE	V	0.9481	0.9367	0.9102	0.9558	0.9842	0.9728	**0.9855**
	S	3	2	1	4	6	5	**7**
RMSE	V	0.0246	0.0271	0.0323	0.0226	0.0136	0.0178	**0.0130**
	S	3	2	1	4	6	5	**7**
MAE	V	0.0088	0.0116	0.0171	0.0103	0.0067	0.0075	**0.0048**
	S	4	2	1	3	6	5	**7**
RSR	V	0.2279	0.2515	0.2997	0.2101	0.1258	0.1648	**0.1205**
	S	3	2	1	4	6	5	**7**
WMAPE	V	0.0116	0.0154	0.0227	0.0136	0.0089	0.0099	**0.0064**
	S	4	2	1	3	6	5	**7**
Total score		23	14	7	26	42	35	**49**

Note: V = Value, S = Score, Bold values indicate best-fitted results.

Table 4. Results for the testing dataset (PR estimation).

Index/Particulars		FFNN	ELM	LR	GBR	DTR	KNR	ENSM
R^2	V	0.9451	0.9326	0.9072	0.9486	0.9625	0.9665	**0.9755**
	S	3	2	1	4	5	6	**7**
WI	V	0.9856	0.9823	0.9750	0.9864	0.9904	0.9911	**0.9937**
	S	3	2	1	4	5	6	**7**
NSE	V	0.9451	0.9326	0.9072	0.9484	0.9625	0.9660	**0.9755**
	S	3	2	1	4	5	6	**7**
RMSE	V	0.0256	0.0284	0.0333	0.0248	0.0212	0.0202	**0.0171**
	S	3	2	1	4	5	6	**7**
MAE	V	0.0091	0.0120	0.0174	0.0110	0.0093	0.0085	**0.0059**
	S	5	2	1	3	4	6	**7**
RSR	V	0.2343	0.2596	0.3046	0.2271	0.1937	0.1845	**0.1566**
	S	3	2	1	4	5	6	**7**
WMAPE	V	0.0120	0.0159	0.0231	0.0145	0.0122	0.0112	**0.0078**
	S	5	2	1	3	4	6	**7**
Total score		25	14	7	26	33	42	**49**

Note: V = Value, S = Score, Bold values indicate best-fitted results.

Table 5. Results for the training dataset (MHS estimation).

Index/Particulars		FFNN	ELM	LR	GBR	DTR	KNR	ENSM
R^2	V	0.9941	0.9979	0.9687	0.9953	0.9951	0.9985	**0.9991**
	S	2	5	1	4	3	6	**7**
WI	V	0.9985	0.9995	0.9922	0.9988	0.9988	0.9996	**0.9998**
	S	2	5	1	4	3	6	**7**
NSE	V	0.9942	0.9979	0.9693	0.9953	0.9952	0.9986	**0.9991**
	S	2	5	1	4	3	6	**7**
RMSE	V	0.0138	0.0083	0.0317	0.0124	0.0126	0.0069	**0.0055**
	S	2	5	1	4	3	6	**7**
MAE	V	0.0095	0.0051	0.0216	0.0085	0.0086	0.0039	**0.0034**
	S	2	5	1	4	3	6	**7**
RSR	V	0.0764	0.0459	0.1751	0.0682	0.0693	0.0378	**0.0304**
	S	2	5	1	4	3	6	**7**
WMAPE	V	0.0307	0.0167	0.0702	0.0277	0.0280	0.0126	**0.0110**
	S	2	5	1	4	3	6	**7**
Total score		14	35	7	28	21	42	**49**

Note: V = Value, S = Score, Bold values indicate best-fitted results.

Table 6. Results for the testing dataset (MHS estimation).

Index/Particulars		FFNN	ELM	LR	GBR	DTR	KNR	ENSM
R^2	V	0.9940	0.9977	0.9675	0.9945	0.9921	0.9980	**0.9985**
	S	3	5	1	4	2	6	**7**
WI	V	0.9985	0.9994	0.9917	0.9986	0.9980	0.9995	**0.9996**
	S	3	5	1	4	2	6	**7**
NSE	V	0.9940	0.9977	0.9674	0.9945	0.9921	0.9980	**0.9985**
	S	3	5	1	4	2	6	**7**
RMSE	V	0.0137	0.0084	0.0318	0.0131	0.0156	0.0079	**0.0068**
	S	3	5	1	4	2	6	**7**
MAE	V	0.0094	0.0052	0.0214	0.0089	0.0107	0.0044	**0.0040**
	S	3	5	1	4	2	6	**7**
RSR	V	0.0775	0.0477	0.1805	0.0741	0.0887	0.0451	**0.0387**
	S	3	5	1	4	2	6	**7**
WMAPE	V	0.0310	0.0171	0.0704	0.0293	0.0353	0.0146	**0.0130**
	S	3	5	1	4	2	6	**7**
Total score		21	35	7	28	14	42	**49**

Note: V = Value, S = Score, Bold values indicate best-fitted results.

To facilitate a rapid evaluation of outcomes, a score was assigned to each index, with a maximum value of 7 representing the total number of employed/developed models and a minimum value of 1. The results of score analysis are also tabulated in Tables 3–6. Notably, the higher the total score, the better the model is. Moreover, the accuracy matrix and scatter plot are presented in Figures 7–10, respectively. An accuracy matrix provides multiple statistical variables that make it possible to the estimation of predictive efficiency quickly. Notably, Figures 9 and 10 shows scatter plots of the best three performing models (as per RMSE index) for each case of PR and MHS estimations. Moreover, error between the actual and estimated values of PR and MHS parameters are illustrated in Figures 11 and 12, respectively.

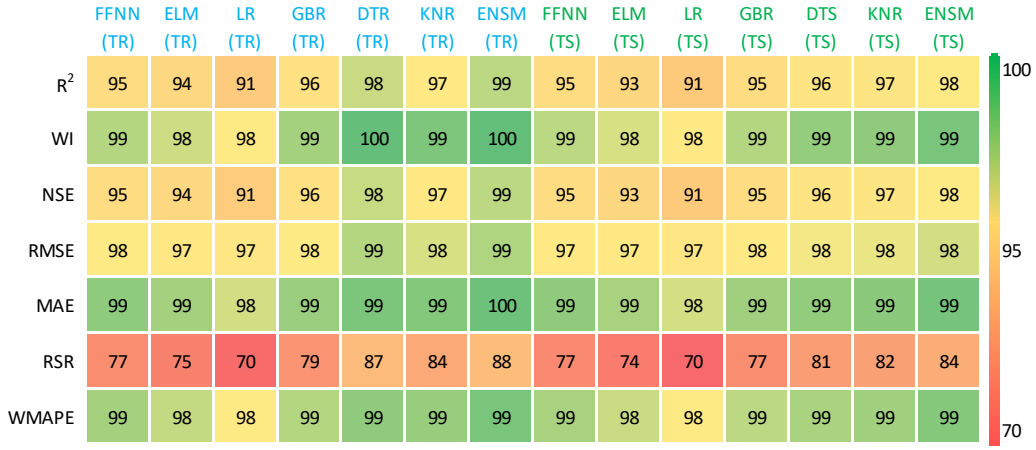

Figure 7. Accuracy matrix for PR estimation.

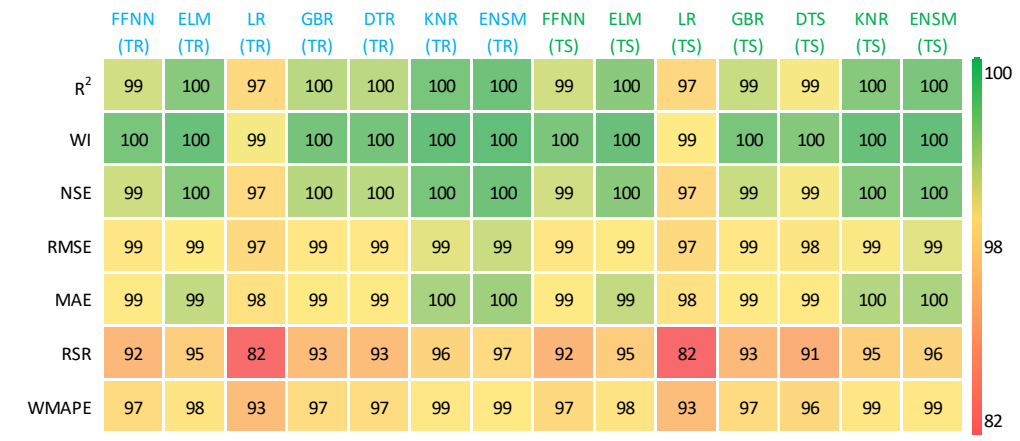

Figure 8. Accuracy matrix for MHS estimation.

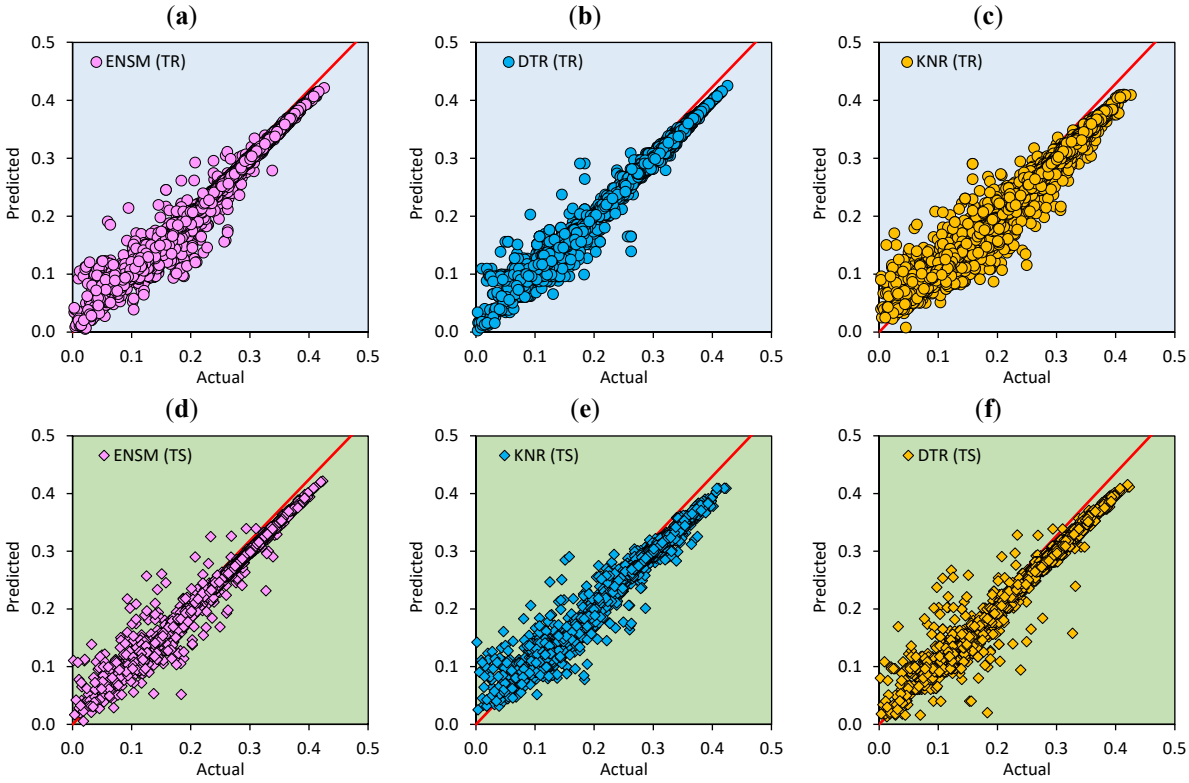

Figure 9. Scatter plots of best three models of PR estimation (**a**–**c**) training and (**d**–**f**) testing phases.

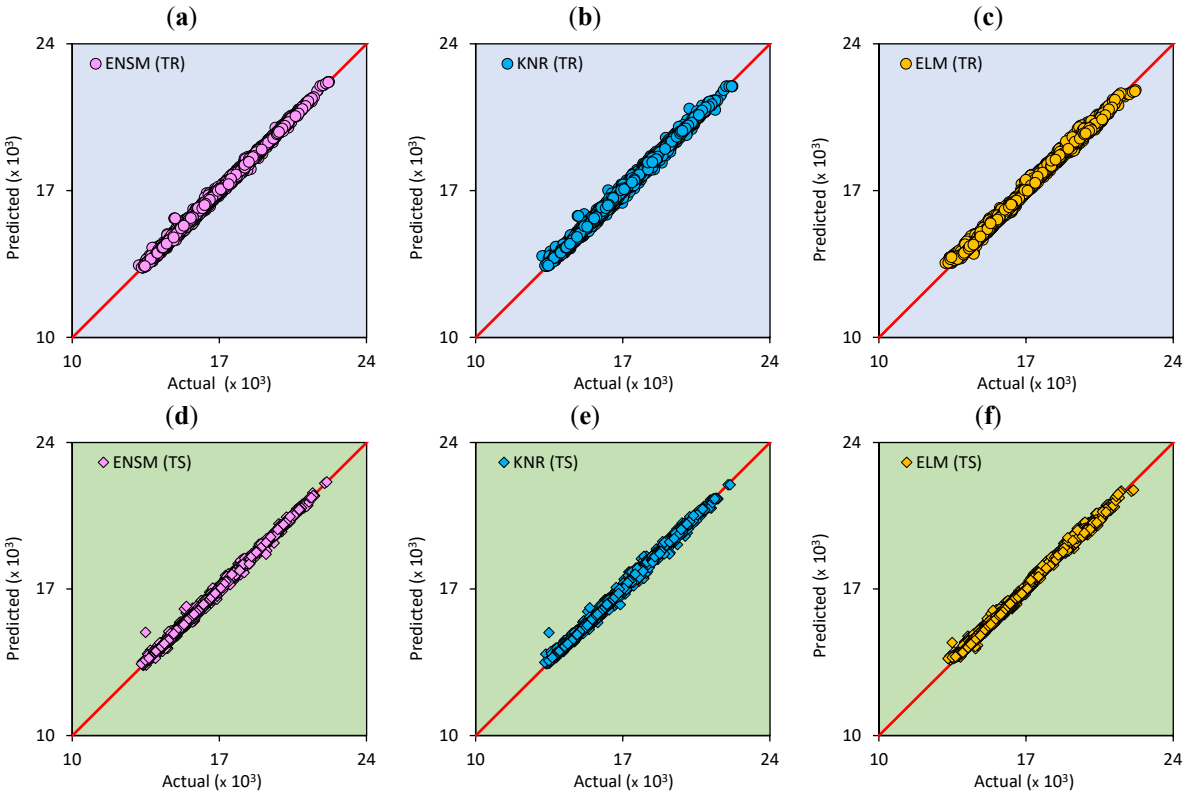

Figure 10. Scatter plots of best three models of MHS estimation (**a**–**c**) training and (**d**–**f**) testing phases.

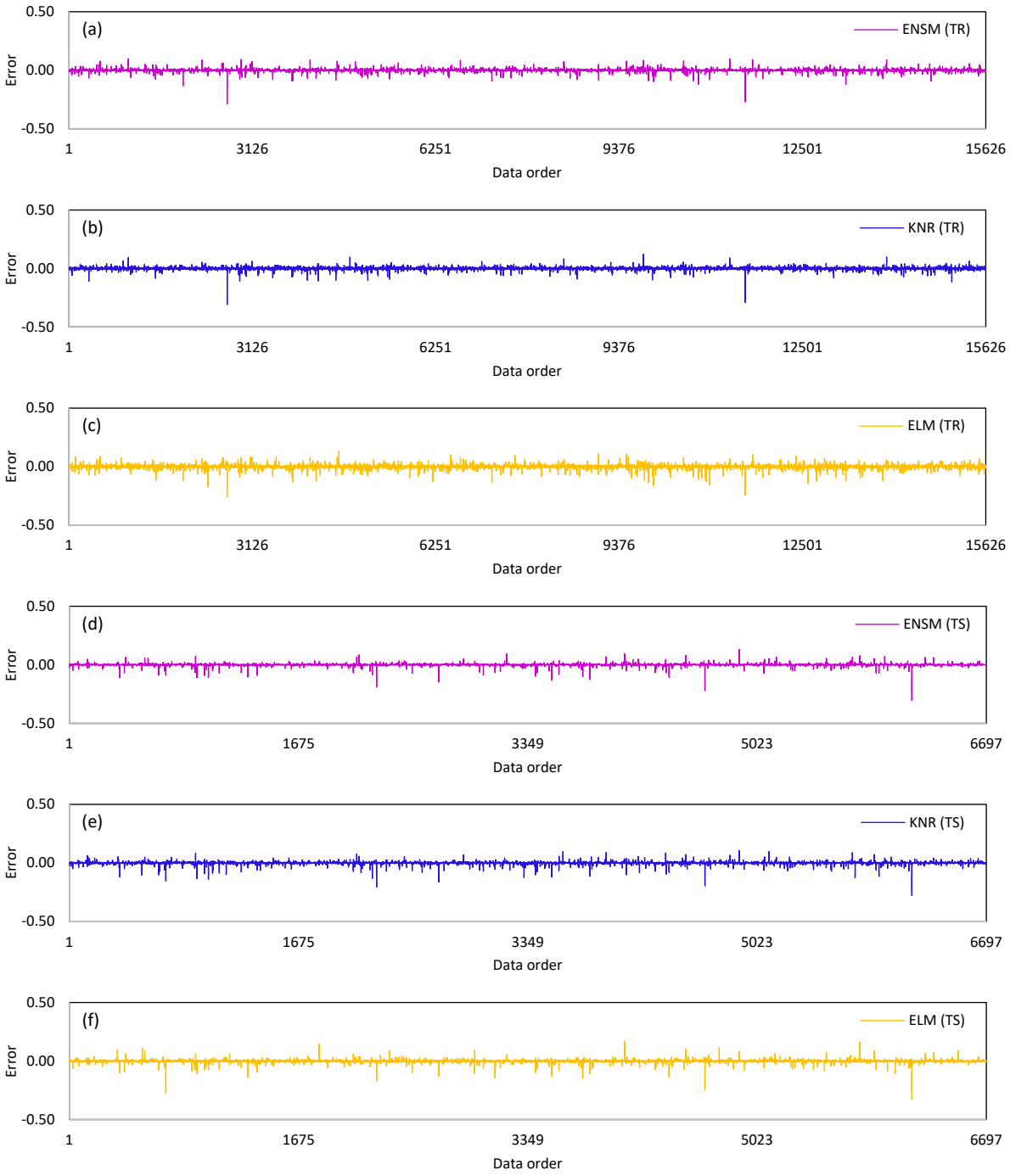

Figure 11. Error plot between the actual and estimated values of PR estimation (**a**–**c**) training and (**d**–**f**) testing phases.

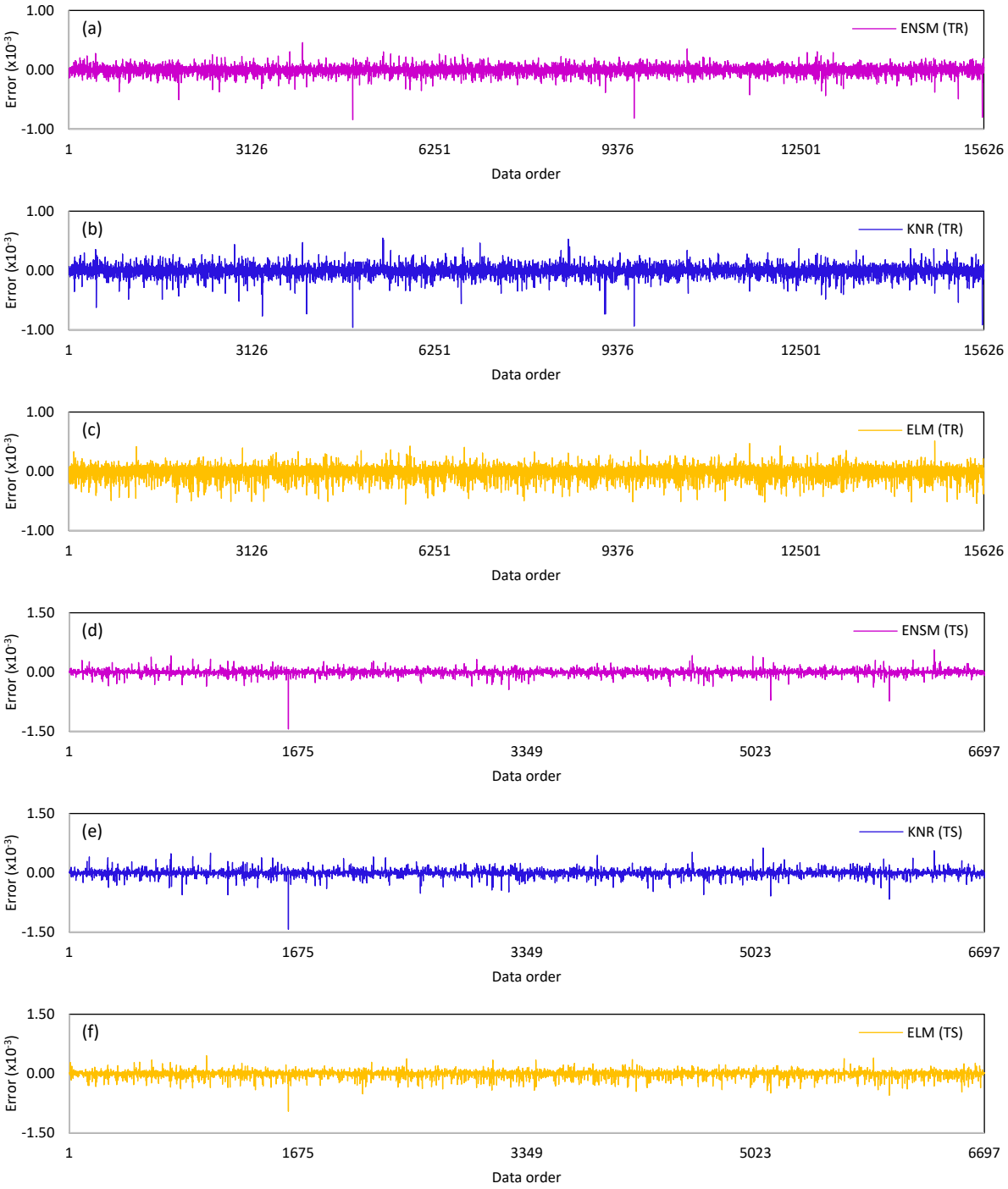

Figure 12. Error plot between the actual and estimated values of MHS estimation (**a**–**c**) training and (**d**–**f**) testing phases.

5.2. Discussion of Results

According to the outcomes, it is seen that all the employed/developed paradigms can achieved (except for LR) a healthy precision in estimating the PR and MHS in casing collapse hazard. The developed models were evaluated for the prediction of PR and MHS in casing collapse assessment case using R^2, WI, NSE, RMSE, MAE, RSR, and WMAPE indices. The results obtained for error measuring indices RMSE, WI, RSR, WMAPE, and NSE showed no ambiguity because the parameters followed the expected patterns. According to the RMSE index, the three most effective models for PR estimation are ENSM, DTR, and KNR; for MHS estimation, the three most effective models are ENSM, KNR, and ELM. In all cases, the maximum predictive efficiency was achieved by the proposed stacking ENSM paradigm.

According to the overall results of score analysis (see Table 7 and Figure 13), the maximum score (i.e., 98 for both PR and MHS prediction) relates to the proposed ENSM paradigm. Also, the final scores of the FFNN, ELM, LR, GBR, DTR and KNR were found to be 48 and 35, 28 and 70, 14 and 14, 52 and 56, 75 and 35, and 77

and 84, of PR and MHS estimations. respectively. These results indicate that the LR is the least-effective model in all cases of PR and MHS estimations. However, to better demonstrate the results of score analysis, stacked bar plot is presented in Figure 13. Moreover, to investigate the reliability of the developed/ employed models, sensitivity analysis (SA) was performed. Notably, SA is used to evaluate the relative influence of the independent variables on the output. For this purpose, the Cosine amplitude method (CAM) was used [44]. To perform SA, the strength of relation (R_S) of input parameters D, DTC, DTS, RHOB, and PP in predicting the PR and MHS were determined for the actual data and ENSM model and the results of which are illustrated in Figure 14. Note that the performance of the testing dataset is only presented. As can be seen, the DTS is the most influential parameter on the PR, followed by DTC, RHOB, D and PP. For the MHS, it has been found that the RHOB is the most influential variable, followed by D, DTC, DTS and PP. It is also worth noting that the proposed ENSM model almost modelled the actual output in predicting the PR and MHS in casing collapse hazard.

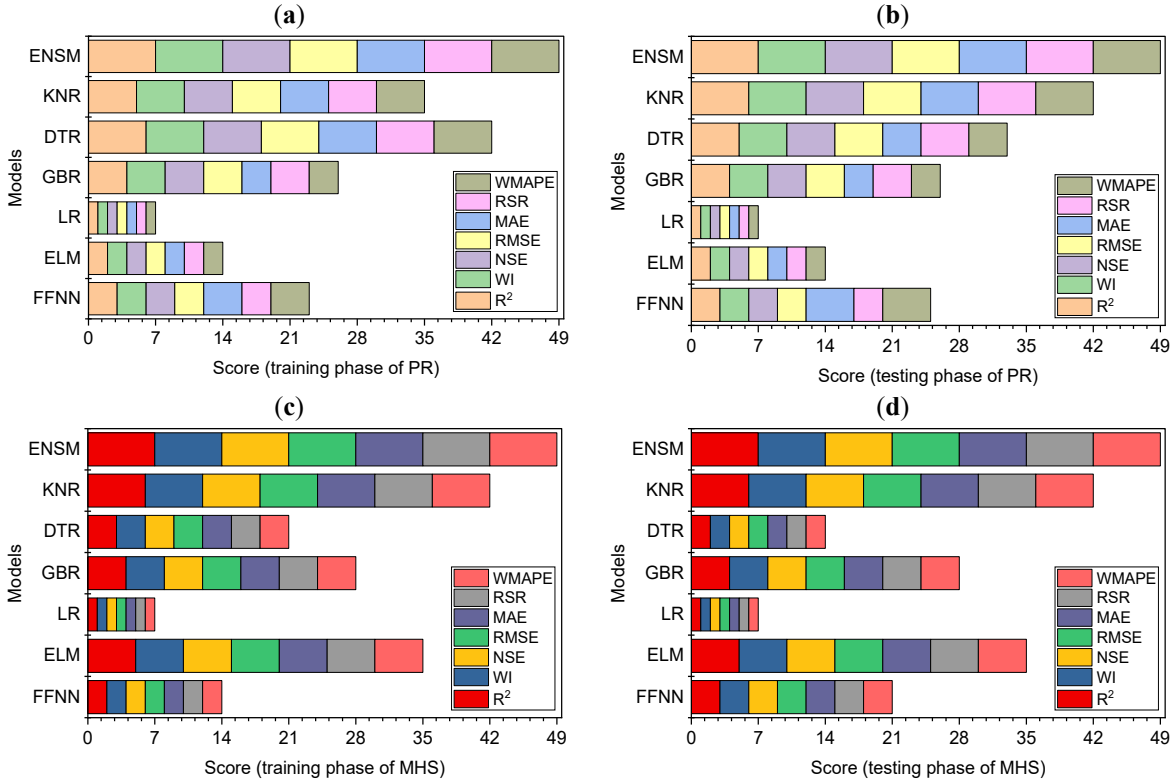

Figure 13. Stacked bar plot of scores for (**a**) PR-training; (**b**) PR-testing, (**c**) MHS-training and (**d**) MHS-testing.

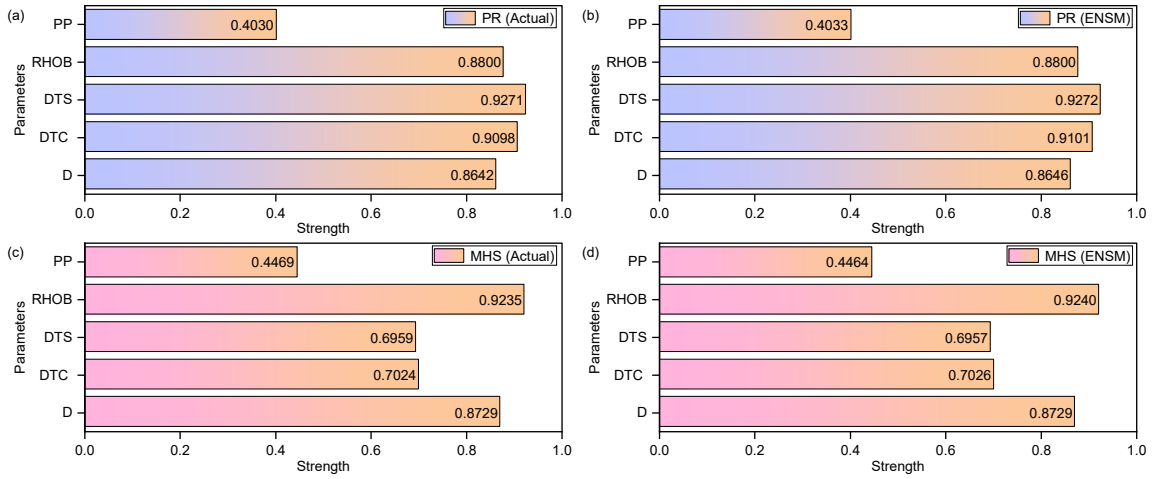

Figure 14. Results of SA for (**a**) PR and (**c–d**) MHS predictions (testing phase).

Table 7. Score summary of PR and MHS estimations.

Subset	FFNN	ELM	LR	GBR	DTR	KNR	ENSM
Training (PR)	23	14	7	26	42	35	**49**
Testing (PR)	25	14	7	26	33	42	**49**
Training (MHS)	14	35	7	28	21	42	**49**
Testing (MHS)	21	35	7	28	14	42	**49**
Training + Testing (PR)	48	28	14	52	75	77	**98**
Training + Testing (MHS)	35	70	14	56	35	84	**98**

Note: Bold values indicate best results.

Notably, due to the compositional differences in rock type, the PR fluctuates in the subsurface. The ductile salt formations, which have a high strain for a provided degree of tension, have a higher propensity for creep than some other rock formations, and may harm deep subterranean structures, including cased wellbores. Hooke's law postulates that the magnitude of strain experienced by a rock formation or cemented casing string is directly proportional to the magnitude of tension exerted on the material, provided that the material remains within its elastic limit. As a result, to determine the strain experienced by sub-surface structures, the stress field must be known. Thus, the MHS is an important parameter for geotechnical modelling as well as wellbore stability optimization. This kind of study is essential for directed wellbore trajectory planning, subsurface fluid injection, and hydraulic fracture program design. So, PR and MHS are the objective functions of the well-log dataset examined, for example, the Marun oil field wellbore. Curves of PR vs. wellbore depth tend to exhibit dramatic leaps at lithology change locations, i.e., formation borders, especially when the juxtaposed rocks have differing geotechnical characteristics. Sharp changes in PR values, for example, are characteristic of salt-anhydride and salt-marl formation interfaces. Significant discrepancies in PR values between two layers with varying creep potentials generate significant shear stress at their interfaces that might lead to failure. These naturally shear stresses tend to concentrate at formation interfaces, where they have a direct influence on the cement sheath as well as steel casing of wellbores that pierce them. Although PR and MHS are not directly connected, it can be demonstrated that at most sub-surface places where PR changes exist, concomitant changes in MHS also take place by superimposing the curves vs. depth. These crucial sub surfaces should be regarded as more vulnerable to casing failure.

6. Summary and Conclusions

This study proposes an efficient meta-ensemble paradigm for modelling the PR and MHS in casing collapse hazard, a geo-mechanical approach to casing collapse prediction in oil and gas wells. Specifically, stacking EMSM paradigm was developed and its performance was compared with six other paradigms including FFNN, ELM, LR, GBR, DTR, and KNR. A mapping function was developed using these prediction models to evaluate the PR and MHS using five influential parameters viz., D, DTC, DTS, RHOB, and PP. For this purpose, a sum of 22,323 data was collected from the literature and was divided into training and testing subsets for model construction and valuation, respectively. The proposed stacking ensemble model enhances predictive performance by integrating the strengths of four base models, thereby reducing individual model bias and variance. By employing the RFR as the meta-learner, the framework effectively captures complex nonlinear relationships and improves generalization capability, leading to more robust and reliable predictions.

Based on the performance indices, the maximum predictive efficiency was achieved by the proposed stacking ENSM paradigm with R^2 values of 0.9855 and 0.9755 for PR prediction, and 0.9991 and 0.9985 for MHS prediction during the training and testing phases, respectively. These results indicate strong model stability, with no significant variances, abnormal values, or overfitting-related deviations observed. The score-based analysis also confirmed that the stacking ENSM paradigm is more efficient once compared to others developed/employed models. Overall, the proposed ENSM paradigm seems to be an effective method for estimating PR and MHS in casing collapse hazard.

The proposed ENSM paradigm has the following advantages: (a) simple architecture; (b) better predictive performance compared to standalone models; (c) robustness, and (d) easy implementation. Notwithstanding these benefits, the exploration of the hyper-parameter space remains a formidable challenge in ensemble-based modelling, necessitating numerous runs and a trial-and-error approach to arrive at the optimal model. On the contrary, even though this study was performed using a large database, the proposed approach should be validated by solving other engineering problems. Thus, the future work should include: (a) implementation and validation of the proposed approach in other fields; (b) a comparative analysis of the outcomes produced by alternative ensemble learning techniques (e.g., boosting and bagging); (c) integration of optimization algorithms to eliminate the need for iterative trial-and-error processes during optimal model construction through automated hyper-

parameter exploration; and (d) utilization of dimension reduction techniques to reduce computation cost. Nevertheless, the ENSM paradigm that has been suggested can be regarded as a valuable framework for assisting professionals and engineers in evaluating the potential for enclosure failure in the context of careful well design and operation procedures.

Supplementary Materials

The additional data and information can be downloaded at: https://media.sciltp.com/articles/others/260403 1724062510/BCI-25120128-Author-Data-from-Mohamadian-et-al.-2021-V2.xlsx. Table S1: 22323 Data Records for Marun Oil Field Well MN#413.

Author Contributions

A.B.: conceptualization, methodology, software validation, writing—original draft preparation, and writing—review; N.K.: data curation and writing—original draft preparation. All authors have read and agreed to the published version of the manuscript.

Institutional Review Board Statement

Not applicable.

Informed Consent Statement

Not applicable.

Data Availability Statement

The datasets can be obtained from the work of Mohamadian et al. [2]. The same is also attached as a supplementary material.

Conflicts of Interest

The authors declare no conflict of interest.

Use of AI and AI-Assisted Technologies

During the preparation of this work, the authors used AI-assisted tools for grammatical corrections. After using these tools, the authors reviewed and edited the content as needed and take full responsibility for the content of the published article."

References

1. Bradley, W.B. Failure of inclined boreholes. *J. Energy Resour. Technol.* **1979**, *101*, 232–239.
2. Mohamadian, N.; Ghorbani, H.; Wood, D.A.; et al. A geomechanical approach to casing collapse prediction in oil and gas wells aided by machine learning. *J. Pet. Sci. Eng.* **2021**, *196*, 107811.
3. Willson, S.M.; Fossum, A.F.; Fredrich, J.T. Assessment of salt loading on well casings. *SPE/IADC Drill. Complet.* **2003**, *18*, 13–21.
4. Gao, D.L.; Zheng, C.K.; Tan, C.J. Numerical simulation of external pressure distribution of casing string with wear in creep formation. *J. China Univ. Pet.* **2007**, *31*, 56–61.
5. Hu, B.; Xu, Z. Casing failure mechanisms and protection measures of oil and water wells in Daqing Oilfield. *Drill. Prod. Technol.* **1998**, *20*, 95–99.
6. Hu, C.; Ai, C.; Tao, F.; et al. Optimization of well completion method and casing design parameters to delay casing impairment caused by formation slippage. In Proceedings of the SPE/IADC Middle East Drilling Technology Conference and Exhibition, Abu Dhabi, UAE, 26–28 January 2016.
7. Jiang, K.; Li, Q.; Chen, Y.; et al. Influence of cementing quality on casing failures in horizontal shale gas wells. *Nat. Gas Ind.* **2015**, *35*, 77–82.
8. Zhou, X.; He, S.; Tang, M.; et al. Mechanism of collapse failure and analysis of yield collapse resistance of casing under combined load. *Eng. Struct.* **2019**, *191*, 12–22.
9. Liu, X.; Yang, X.; Wang, J. A nonlinear creep model of rock salt and its numerical implement in FLAC 3D. *Adv. Mater. Sci. Eng.* **2015**, *2015*, 285158.

10. Wang, H.; Samuel, R. 3D geomechanical modeling of salt-creep behavior on wellbore casing for presalt reservoirs. *SPE Drill. Complet.* **2016**, *31*, 261–272.
11. Firme, P.A.L.P.; Roehl, D.; Romanel, C. An assessment of the creep behaviour of Brazilian salt rocks using the multi-mechanism deformation model. *Acta Geotech.* **2016**, *11*, 1445–1463.
12. Tong, H.; Guo, D.; Zhu, X. Application of multiphysics coupling FEM on open wellbore shrinkage and casing remaining strength in an incomplete borehole in deep salt formation. *Math. Probl. Eng.* **2015**, *2015*, 575492.
13. Hedayatikhah, S.; Abdideh, M. 3D Geomechanical modeling of casing collapse in plastic formations (Cap Rock of Hydrocarbon Reservoir). *Nat. Resour. Res.* **2019**, *28*, 273–286.
14. Salehi, S.; Hareland, G.; Dehkordi, K.K.; et al. Casing collapse risk assessment and depth prediction with a neural network system approach. *J. Pet. Sci. Eng.* **2009**, *69*, 156–162.
15. Wang, P.; Zhong, C.; Fan, S.; et al. Prediction of Collapsing Strength of High-Strength Collapse-Resistant Casing Based on Machine Learning. *Processes* **2023**, *11*, 3007.
16. Xue, J. Casing damage classification method using random forest algorithms. *J. Phys. Conf. Ser.* **2020**, *1437*, 012131.
17. Noshi, C.I.; Noynaert, S.F.; Schubert, J.J. Failure predictive analytics using data mining: How to predict unforeseen casing failures? In Proceedings of the Abu Dhabi International Petroleum Exhibition & Conference, Abu Dhabi, UAE, 11–15 November 2018.
18. Nilashi, M.; bin Ibrahim, O.; Ahmadi, H.; et al. An analytical method for diseases prediction using machine learning techniques. *Comput. Chem. Eng.* **2017**, *106*, 212–223.
19. Mosavi, A.; Ozturk, P.; Chau, K. Flood prediction using machine learning models: Literature review. *Water* **2018**, *10*, 1536.
20. Matloob, F.; Ghazal, T.M.; Taleb, N.; et al. Software defect prediction using ensemble learning: A systematic literature review. *IEEE Access* **2021**, *9*, 98754–98771.
21. Lee, J.; Wang, W.; Harrou, F.; et al. Wind power prediction using ensemble learning-based models. *IEEE Access* **2020**, *8*, 61517–61527.
22. Lee, J.; Wang, W.; Harrou, F.; et al. Reliable solar irradiance prediction using ensemble learning-based models: A comparative study. *Energy Convers. Manag.* **2020**, *208*, 112582.
23. Quan, V.; Do, H.Q. Prediction of California bearing ratio (CBR) of stabilized expansive soils with agricultural and industrial waste using light gradient boosting machine. *J. Sci. Transp. Technol.* **2021**. https://doi.org/10.58845/jstt.utt.2021.en3.
24. Khatti, J.; Grover, K.S. Relationship Between Index Properties and CBR of Soil and Prediction of CBR. In *Transportation and Environmental Geotechnics*; Springer: Singapore, 2021; pp. 171–185.
25. Iqbal, M.; Onyelowe, K.C.; Jalal, F.E. Smart computing models of California bearing ratio, unconfined compressive strength, and resistance value of activated ash-modified soft clay soil with adaptive neuro-fuzzy inference system and ensemble random forest regression techniques. *Multiscale Multidiscip. Model. Exp. Des.* **2021**, *4*, 207–225.
26. Zhang, W.; Li, H.; Han, L.; et al. Slope stability prediction using ensemble learning techniques: A case study in Yunyang County, Chongqing, China. *J. Rock Mech. Geotech. Eng.* **2022**, *14*, 1089–1099.
27. Ullah, H.S.; Khushnood, R.A.; Farooq, F.; et al. Prediction of compressive strength of sustainable foam concrete using individual and ensemble machine learning approaches. *Materials* **2022**, *15*, 3166.
28. Song, Y.; Zhao, J.; Ostrowski, K.A.; et al. Prediction of compressive strength of fly-ash-based concrete using ensemble and non-ensemble supervised machine-learning approaches. *Appl. Sci.* **2021**, *12*, 361.
29. Li, Q.-F.; Song, Z.-M. High-performance concrete strength prediction based on ensemble learning. *Constr. Build. Mater.* **2022**, *324*, 126694.
30. Li, Q.; Song, Z. Prediction of compressive strength of rice husk ash concrete based on stacking ensemble learning model. *J. Clean. Prod.* **2023**, *382*, 135279.
31. Ikeagwuani, C.C.; Nwonu, D.C. Statistical analysis and prediction of spatial resilient modulus of coarse-grained soils for pavement subbase and base layers using MLR, ANN and Ensemble techniques. *Innov. Infrastruct. Solut.* **2022**, *7*, 273.
32. Raheem, Z.; Mohammed, Z.; Barzan, Z.; et al. Hybrid Data-Driven and Explainable Modeling of Compressive Strength in GGBFS–MRP Concrete with Environmental Optimization. *Bull. Comput. Intell.* **2026**, *2*, 13–30.
33. Benzaamia, A.; Ghrici, M.; Rbouh, R.; et al. Prediction of chloride resistance level in concrete using optimized tree-based machine learning Models. *Bull. Comput. Intell.* **2025**, *1*, 104–117.
34. Sarhadi, A.; Ravanshadnia, M.; Monirabbasi, A.; et al. Optimizing concrete crack detection: An attention-based swin u-net approach. *IEEE Access* **2024**, *12*, 77575–77585.
35. Savvides, A.A.; Papadopoulos, L. A neural network approach for the reliability analysis on failure of shallow foundations on cohesive soils. *Int. J. Geo-Eng.* **2024**, *15*, 15.
36. Silewu, K.; Kahanji, C.; Simwanda, L.; et al. Intelligent Data Driven Ensemble Approaches for Bending Strength Prediction of Ultra-High Performance Concrete Beams. *Bull. Comput. Intell.* **2025**, *1*, 31–52.
37. Shahin, M.A.; Jaksa, M.B.; Maier, H.R. State of the art of artificial neural networks in geotechnical engineering. *Electron. J. Geotech. Eng.* **2008**, *8*, 1–26.

38. Muhammed, A.M.; Omer, M.A.I.; Haider, R.S.; et al. Predicting the Compressive Strength of Fly Ash Composite Foam Concrete Using Artificial Neural Networks and Soft Computing Techniques. *Bull. Comput. Intell.* **2026**, *2*, 83–102.
39. Huang, G.B.; Zhu, Q.Y.; Siew, C.K. Extreme learning machine: Theory and applications. *Neurocomputing* **2006**, *70*, 489–501. https://doi.org/10.1016/j.neucom.2005.12.126.
40. Spross, J.; Johansson, F. When is the observational method in geotechnical engineering favourable? *Struct. Saf.* **2017**, *66*, 17–26.
41. Shahriar, K.; Sharifzadeh, M.; Hamidi, J.K. Geotechnical risk assessment based approach for rock TBM selection in difficult ground conditions. *Tunn. Undergr. Space Technol.* **2008**, *23*, 318–325.
42. Ansari, S.S.; Ansari, M.A.; Ibrahim, S.M. Explainable Predictive Modelling of Sustainable Slag–Fly Ash Based Geopolymer Concrete with Life Cycle and Carbon-Neutrality Assessment. *Bull. Comput. Intell.* **2026**, *2*, 54–82.
43. Fehrmann, L.; Lehtonen, A.; Kleinn, C.; et al. Comparison of linear and mixed-effect regression models and a k-nearest neighbour approach for estimation of single-tree biomass. *Can. J. For. Res.* **2008**, *38*, 1–9.
44. Jong, Y.-H.; Lee, C.-I. Influence of geological conditions on the powder factor for tunnel blasting. *Int. J. Rock Mech. Min. Sci.* **2004**, *41*, 533–538.